Optics Letters

Hierarchically structuring and synchronous photoreduction of graphene oxide films by laser holography for supercapacitors

Xiu-Yan Fu,[1] Yong-Lai Zhang,[1,*] Hao-Bo Jiang,[3] Dong-Dong Han,[1] Yu-Qing Liu,[1] Hong Xia,[1] and Hong-Bo Sun[2]

[1]State Key Laboratory of Integrated Optoelectronics, College of Electronic Science and Engineering, Jilin University, Changchun 130012, China
[2]State Key Laboratory of Precision Measurement Technology and Instruments, Department of Precision Instrument, Tsinghua University, Beijing 100084, China
[3]Key Laboratory of Bionic Engineering (Ministry of Education), Jilin University, Changchun 130022, China
*Corresponding author: yonglaizhang@jlu.edu.cn

Received 27 September 2018; revised 28 February 2019; accepted 1 March 2019; posted 4 March 2019 (Doc. ID 346318); published 26 March 2019

Herein, we report a simple laser holography technology for hierarchically structuring and synchronous photoreduction of graphene oxides (GO), toward the development of efficient graphene-based electrodes for supercapacitor applications in cost effectively manners. Hierarchical micro-nanostructures, formed due to laser treatment induced photoreduction and ablation effect. Interestingly, both the morphology and reduction degree of the laser holography reduced GO (LHRGO) show strong dependence on the laser intensity, providing the feasibility for controlling the micro-nanostructures, chemical composition, and the conductivity of the graphene electrodes. Furthermore, the supercapacitors based on LHRGO show higher capacitance values and better electrochemical performance compared to that based on thermal reduced GO (TRGO) of same reduction level. Photoredution and micro-nanostructuring of GO using laser holography may hold great promise for production of effective carbon-based electrodes towards practical applications in energy storage devices.

https://doi.org/10.1364/OL.44.001714

Today energy storage devices play a very important role in our daily life. Especially triggered by the advancement of portable and wearable electronic devices, there is a growing trend for developing high-quality energy storage systems that have a large energy capacity and are small in size and light in weight. Thus, as two typical kinds of energy storage devices, batteries and supercapacitors have been intensively researched in recent years. Compared with batteries, supercapacitors [1–7] have demonstrated higher power density and longer cycle life. Nevertheless, the working mechanism, which depends on the rapid physical adsorption on the electrode-electrolyte interface and fast reversible redox reaction at the surface of the electrode materials, also results in relatively lower energy density than that of battery. To make supercapacitors workable in real applications, it is imperative to enhance its energy density. Among different strategies, selecting an appropriate electrode material is key. Typically, an efficient electrode material needs to meet the demands of high specific surface areas, good conductivity, good ion transport channels and excellent mechanical/chemical stability. Graphene [8–15] that possesses superior electrical conductivity, flexibility, mechanical strength, and high surface area (over 2600 $m^2 g^{-1}$) perfectly satisfied all of the above requirements. As reported in a comprehensive review published recently, graphene has been considered favorable electrode materials for energy applications and storage [16]. To prepare graphene electrodes in cost-effective manner, graphene oxide (GO) [17–19] prepared by simple chemical oxidation of natural graphite have been proven an ideal precursor for mass production of graphene-related materials. However, during the chemical oxidation process, many oxygen-containing groups (OCGs) have been introduced into the GO sheets, which destroy the planar sp^2 carbon network. The presence of OCGs makes GO insulating, which limits its applications as electrodes. Therefore, further reduction treatments must be carried out to recover its electrical conductivity.

At present, in order to remove the OCGs and partially restore sp^2 carbon network, the commonly used methods to reduce GO include chemical reduction [20], thermal reduction [21], and photoreduction [22]. Among these approaches, chemical reduction always involves the use of toxic reducing agents, which is inapplicable for large-scale production. As an alternative, thermal reduction of GO is also workable for effective removal of OCGs. However, it needs high temperature and should be protected by inert gas, which greatly hinder its practical application. As compared with the above-mentioned methods, laser-mediated photoreduction of GO has revealed distinct advantages. Laser reduction of GO has been considered as a green route for GO reduction because it does not need any additional chemical agents or high temperature. Also, it permits refined control over the reduction degree, oxygen residual, conductivity and the exfoliated micronanostructures, revealing great potential

for developing graphene-based devices. As typical examples, Gao *et al.* reported high performance micro-supercapacitors based on reduced GO (RGO) films fabricated by direct laser writing of hydrated GO films [23]; EI-Kady *et al.* reported the flexible graphene-based electrochemical capacitors by laser scribing technology [24]. In these works, laser mediated photoreduction strategies have demonstrated distinct advantages in flexible patterning and inducing porous structures, which contributes to the device fabrication and function promotion. However, for photoreduction of GO, the formation of micronanostructures is generally uncontrollable. Research works with respect to controllable laser reduction and structuring of GO-based supercapacitor electrodes that demonstrate periodic hierarchical micronanostructures are still rare.

In this work, we report the hierarchical structuring and synchronous photoreduction of GO using nanosecond laser holography technology toward the development of high efficiency supercapacitor electrodes. The laser treatments enable precise control over the hierarchical micro-nanostructures, chemical composition and the conductivity of the resultant graphene electrodes. With the help of laser holography technology, hierarchical micro-nanostructures, including microscale gratings and layered nanoporous structures, can form due to laser photoreduction and ablation effects. Importantly, the supercapacitors based on these laser holography reduced GO (LHRGO) electrodes show much higher capacitance values and better electrochemical performance than that based on thermal reduced GO (TRGO, 200°C for 30 min named TRGO1; 200°C for 1 h named TRGO2) electrodes of same reduction level. Furthermore, we demonstrated that hierarchically structured RGO electrodes fabricated by laser holography may hold great promise for developing carbon-based energy storage devices.

Multibeam interference lithography has been widely used in rapid, mask-free, and large area micronano-fabrication, especially in 2D gratings and 3D photonic crystals [25]. Pioneer works reported by our group [26] and others have proven its value in developing biomimetic structures and surfaces. In this work, we focused on the outstanding electrochemical performance of LHRGO. Making full use of laser holography treatment, the hierarchical micro-nanostructures, chemical composition and the conductivity can be precisely controlled. Figure 1(a) shows the schematic illustration of laser holography fabrication system. The laser beam was first split into two equal-intensity beams, and then the acquired two beams were guided to interfere right on the surface of a GO film. In this way, LHRGO films had been successfully prepared. First, we study the microscopic surface morphology of micro-nanostructured LHRGO film. Generally, the period of the grating can be precisely controlled by the following equation:

$$T = \frac{\lambda}{2\sin(\theta/2)}, \tag{1}$$

where T is the period, λ, the laser wavelength and θ is the angle between two beams. We found that the morphology and structure of the LHRGO surface depends on both the grating period and laser power. Here, we have the periodicity of interference grating settled and only modified three different laser power (0.3 W, 0.35 W, and 0.4 W, respectively, before beam splitting) to treat the GO surface. Then, the grating structures with different morphologies have been obtained. Figures 1(b)–1(d) show the scanning electron microscope (SEM) images of the as-obtained LHRGO samples with same period of 2 μm

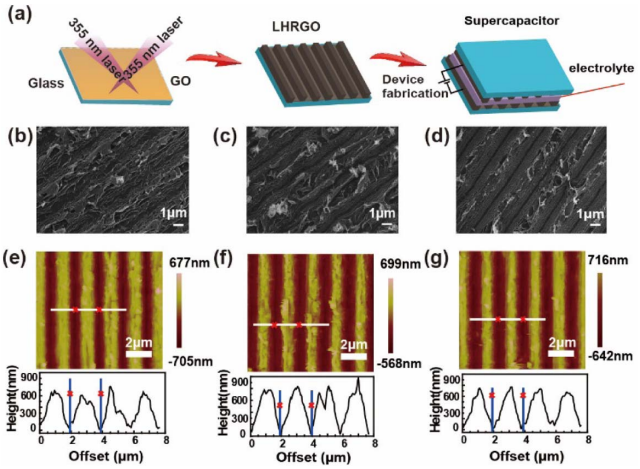

Fig. 1. (a) Schematic illustration for the fabrication process, SEM images of LHRGO1 (b), LHRGO2 (c), and LHRGO3 (d) and AFM image of LHRGO1 (e), LHRGO2 (f), and LHRGO3 (g) and the corresponding height of the surface along with the white line.

fabricated under laser power of 0.3 W [Fig. 1(b)], 0.35 W [Fig. 1(c)], and 0.4 W [Fig. 1(d)], respectively. It can be seen from these images that laser holography treatments under different laser power can induce distinct micronanostructures. The grating structures became clear with the increase of the laser intensity. The formation of the periodic structure can be attributed to the periodic light field patterns generated by the interfered laser beams. In the high intensity region, GO films can be partially ablated. On the contrary, in the region of low intensity, RGO can be exfoliated, forming a layered nanostructure due to the emission of gas species. When the laser intensity is relatively low, the ablation effect is not obvious, and thus the resultant grating is not very neat. As the laser intensity increases, the GO grating groove has become clear. It can be observed from the SEM images that all of these samples show obvious hierarchical micro-nanostructures. The laser holography treatment revealed great potential for controllably structuring of GO, hierarchical micro-nanostructures including microscale gratings and layered nanoporous structures can form without the use of any chemicals or shadow masks. On the contrary, the TRGO1 and TRGO2 shows very smooth morphology. In order to further investigate the effect of different laser intensity on the height of the ablated grating structure, we also characterized these samples using atomic force microscopy (AFM). As shown in Figs. 1(e)–1(g), the period of these samples is 2 μm, in good agreement with the SEM results. Moreover, the morphologies are also similar to that shown in the SEM images. From the height diagram of the section obtained from the white line [Figs. 1(e)–1(g)], we found that the heights of the grating are between 600 and 800 nm.

X-ray photoelectron spectroscopy (XPS) was applied to explore the surface chemistry of GO and LHRGO samples. Figure 2(a) shows the C1s spectra of the GO and LHRGO films. The C1s peak of GO could be simply fitted into three peaks at ~284.7, ~286.8, and ~288.2 eV, which could be attributed to C—C (nonoxygenated ring carbon), C—O (hydroxyl and epoxy carbon), and C═O (carbonyl), respectively. There are two obvious peaks at ~286.8 eV and ~288.2 eV, correspond to C—O and C═O, respectively in GO sheet. It is worth noting that these two peaks of shifted to 285.8 eV and 287.8 eV, respectively,

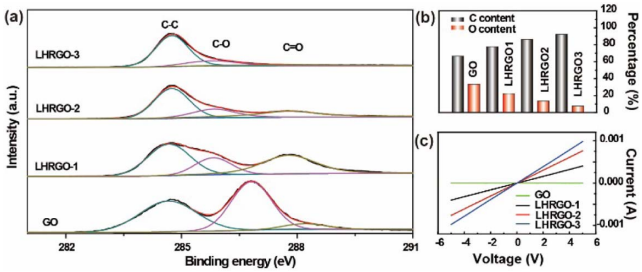

Fig. 2. (a) C1s XPS spectra of go and LHRGO1-3, (b) C, O content of go and LHRGO1-3 and (c) I-V curves of go and LHRGO1-3.

which is due to the deoxidation process. As shown in Fig. 2(b), the oxygen content in the pure GO film is up to 33.49%, and the C/O atom ratio is about 1.98. After laser holography treatments, the peak of C—O and C═O decreased significantly. In detail, when the laser power of 0.3 W was applied to the surface of the GO films, the oxygen content decreased to 22.42%, and the C/O atom ratio became 3.46. When the laser power was further increased to 0.35 W, they further became 13.6% and 6.35; 0.4 W, 7.7%, and 11.98. These results indicated that laser holography treatments can remove most of the OCGs in the GO films, especially when the incident laser power is high. It is clear that OCGs on the surface of the GO seriously hinder the conductivity. Photoreduction induced by laser holography treatment can greatly improve the conductivity of the GO film after reduction. Figure 2(c) shows the I-V curve of LHRGO films, the conductivity of the sample increased along with the increasing C/O ratio. We have measured the surface resistivity of LHRGO1-LHRGO3 samples, they are 2421, 1885 and 1676Ω/□, respectively, which is consistent with the I-V curves. Thus, the chemical composition and the conductivity of the resultant LHRGO films can be preciously controlled by laser holography treatments.

Furthermore, we have fabricated the supercapacitors according to the procedure shown in Figure 1. The electrochemical tests were carried out to characterize device performance. According to the different laser intensity applied on the surface of GO, the resultant graphene films were named LHRGO1 (laser power: 0.3 W), LHRGO2 (laser power: 0.35 W), and LHRGO3 (laser power: 0.4 W), respectively. As a controlled experiment, TRGO with same reduction level were also produced for comparison. All the electrodes were cut into proper pieces (effective area was settled as 1 cm^2). Then, they were assembled into a sandwich structure, consisting of two identical LHRGO or TRGO electrodes with silver wires as electrical leads and gel electrolyte embedded in between. To get a full comparison among these electrodes, we first investigate the effects of laser power on the performance of supercapacitors. Figure 3 shows the Cyclic Voltammetry (CV) plots and Galvano static Charge/Discharge test (GCD) curves of three LHRGO-based supercapacitors. The specific capacitance can be measured by two methods. From CV plots, C_{SC} can be calculated by the following formula:

$$C_{SC} = \frac{\int_{V_L}^{V_H} I\,dv}{SA(V_H - V_L)}, \tag{2}$$

where C_{SC} is the specific capacitance, I is the current density, S, the scan rate, A, the effective area, and $(V_H - V_L)$, the potential

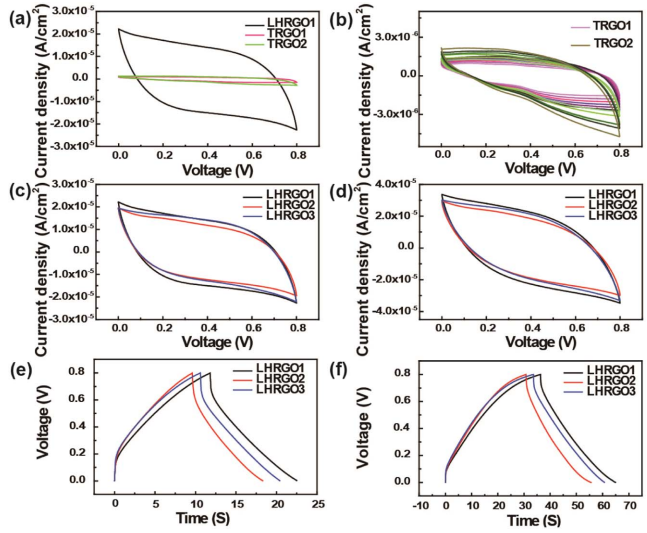

Fig. 3. (a) CV plots (scan rate: 50 mV/s) of LHRGO1, TRGO1, and TRGO2, (b) CV plots of TRGO1 and TRGO2 under different scan rates, CV plots of supercapacitors based on LHRGO1-3 at scan rate of (c) 50 mV/s and (d) 100 mV/s, and GCD curves of supercapacitors based on LHRGO1-3 at current density of (e) 0.01 mA/cm^2 and (f) 0.02 mA/cm^2, respectively.

difference from the beginning of discharge to the end. From GCD curves, C_{SG} can be calculated by the following formula:

$$C_{SG} = \frac{I\Delta t}{A\Delta V}, \tag{3}$$

where C_{SG} is the specific capacitance, Δt, the discharge time, ΔV, the potential difference from the beginning of discharge to the end. Compared to TRGO-based supercapacitor, the CV plots of supercapacitor based on LHRGO1 showed more rectangular shape and bigger integral area due to the presence of the hierarchical structures [Fig. 3(a)]. Although the supercapacitors based on TRGO1 and TRGO2 also showed rectangular shape and acceptable rate performance [Fig. 3(b)], their capacities are much lower than that based on LHRGO electrodes. For CV plots, we selected the same scan rate of 50 mV/s and 100 mV/s, as shown in Figs. 3(c) and 3(d). With the increase of laser power, the specific capacitance was slightly decreased and then recovered. This phenomenon can be attributed to the difference in surface resistivity, surface area, and surface chemical composition. Under higher laser intensity, GO had been reduced more thoroughly. In this condition, more graphene fragments and OCGs were ablated, so the specific capacitance decreased slightly. Nevertheless, photoreduction under higher laser intensity can lead to much higher conductivity, which can promote ion transport. In addition to the surface resistivity, the surface area has been also taken into account. The BET surface areas for LHRGO1 and LHRGO3 have been measured to be 66.1 and 109.4 $m^2\,g^{-1}$, respectively. Therefore, the capacitance of the supercapacitor based on LHRGO3 recovered slightly. We also compared the GCD curves results [see Figs. 3(e) and 3(f)] with current densities of 0.01 and 0.02 mA/cm^2, respectively. The discharge time shows the same tendency with CV plots. It is worth noting that supercapacitor based on LHRGO1 show the best performance among these devices. These results indicate that both the micronanostructures

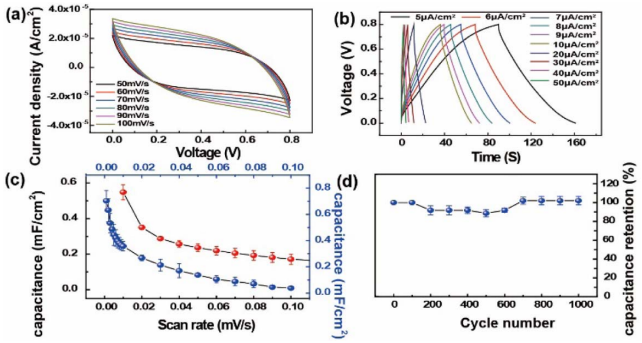

Fig. 4. (a) CV plots (scan rate: 50–100 mV/s) and (b) GCD curves (current density: 5–50 μA/cm^2) and (c) specific capacitance of LHRGO1 based supercapacitor at different scan rates (the blue line) or different current densities (the red line) and (d) specific capacitance retention after 1000 cycles of LHRGO1 based supercapacitor.

and the chemical composition of the RGO electrodes show strong influence on the device performance. Figure 4(a) shows the CV plots of the supercapacitor based on LHRGO1 at a scan rate of 50 mV/s–100 mV/s. Figure 4(b) are GCD curves of supercapacitor based on LHRGO1 at current density of 5–50 μA/cm^2. Figure 4(c) is specific capacitance calculated from different scan rates or current densities. The initial C_{SC} calculated from CV plot (scan rate: 10mV/s) is 0.55 mF/cm^2, and initial C_{SG} calculated from GCD curve (current density: 1 μA/cm^2) is 0.70 mF/cm^2. This is consistent with the previous analysis. Besides, the cycle life is another important index measuring the performance of supercapacitor, which can reflect the stability and practicality of the devices. In Fig. 4(d) we tested the cycle life through GCD test at the current density of 0.02 mA/cm^2. After 1000 cycles, our device stability is fairly good and stable with at least 90% retention of the initial specific capacitance. We believe further exploration in changing period of gratings may further promote the device performance.

In conclusion, we realized the photoreduction and synchronously micro-nanostructuring of GO films for effective production of supercapacitor electrodes using a simple laser holography technology. The as-prepared LHRGO films showed hairy and porous micronanostructures, which greatly promoted ion transport and contributed to the improvement in device performance. Furthermore, the supercapacitors based on LHRGO electrodes showed much higher capacitance values and better electrochemical performance than those based on TRGO electrodes, despite all of these RGO samples showing similar reduction degree. Additionally, we investigated the influence of laser intensity on the photoreduction degree, formation of micronanostructures, and the device performance. Experimental results show that both the morphology and reduction degree of the LHRGO film can be precisely tuned by the laser intensity, providing the feasibility for controlling the micro-nanostructures, chemical composition, and the conductivity of the graphene electrodes. We deem that laser holography technique might emerge as a powerful technology for fabrication of hierarchically structured electrode materials towards a broad range of applications in energy storage devices.

Funding. National Key Research and Development Program of China and National Natural Science Foundation of China (NSFC) (#2017YFB1104300, #61775078, #61590930, #61522503, #61605055).

REFERENCES

1. A. Gonzalez, E. Goikolea, J. A. Barrena, and R. Mysyk, Renew. Sustain. Energy Rev. **58**, 1189 (2016).
2. Z. S. Wu, K. Parvez, X. L. Feng, and K. Mullen, Nat. Commun. **4**, 1463 (2013).
3. J. J. Yoo, K. Balakrishnan, J. S. Huang, V. Meunier, B. G. Sumpter, A. Srivastava, M. Conway, A. L. M. Reddy, J. Yu, R. Vajtai, and P. M. Ajayan, Nano Lett. **11**, 1423 (2011).
4. L. L. Zhang, X. Zhao, M. D. Stoller, Y. W. Zhu, H. X. Ji, S. Murali, Y. P. Wu, S. Perales, B. Clevenger, and R. S. Ruoff, Nano Lett. **12**, 1806 (2012).
5. W. Li, F. Zhang, Y. Q. Dou, Z. X. Wu, H. J. Liu, X. F. Qian, D. Gu, Y. Y. Xia, B. Tu, and D. Y. Zhao, Adv. Energy Mater. **1**, 382 (2011).
6. J. Lao, P. Sun, F. Liu, X. Zhang, C. Zhao, W. Mai, T. Guo, G. Xiao, and J. Albert, Light: Sci. Appl. **7**, 34 (2018).
7. X.-Y. Zhang, S.-H. Sun, X.-J. Sun, Y.-R. Zhao, L. Chen, Y. Yang, W. Lu, and D.-B. Li, Light: Sci. Appl. **5** e16130 (2016).
8. Z.-B. Zheng, J.-T. Li, T. Ma, H.-L. Fang, W.-C. Ren, J. Chen, J.-C. She, Y. Zhang, F. Liu, H.-J. Chen, S.-Z. Deng, and N.-S. Xu, Light: Sci. Appl. **6**, e17057 (2017).
9. P. Kang, K.-H. Kim, H.-G. Park, and S. Nam, Light: Sci. Appl. **7**, 17 (2018).
10. W. Yang, M. Ni, X. Ren, Y. F. Tian, N. Li, Y. F. Su, and X. L. Zhang, Curr. Opin. Colloid Interface Sci. **20**, 416 (2015).
11. L. L. Zhang, R. Zhou, and X. S. Zhao, J. Mater. Chem. **20**, 5983 (2010).
12. Y. L. Shao, M. F. El-Kady, L. J. Wang, Q. H. Zhang, Y. G. Li, H. Z. Wang, M. F. Mousavi, and R. B. Kaner, Chem. Soc. Rev. **44**, 3639 (2015).
13. W. K. Chee, H. N. Lim, Z. Zainal, N. M. Huang, I. Harrison, and Y. Andou, J. Phys. Chem. C **120**, 4153 (2016).
14. J. Yan, Q. Wang, T. Wei, L. L. Jiang, M. L. Zhang, X. Y. Jing, and Z. J. Fan, ACS Nano **8**, 4720 (2014).
15. P. Pachfule, D. Shinde, M. Majumder, and Q. Xu, Nat. Chem. **8**, 718 (2016).
16. A. H. Khan, S. Ghosh, B. Pradhan, A. Dalui, L. K. Shrestha, S. Acharya, and K. Ariga, Bull. Chem. Soc. Jpn. **90**, 627 (2017).
17. Y. X. Xu, C. Y. Chen, Z. P. Zhao, Z. Y. Lin, C. Lee, X. Xu, C. Wang, Y. Huang, M. I. Shakir, and X. F. Duan, Nano Lett. **15**, 4605 (2015).
18. F. Li, X. Jiang, J. J. Zhao, and S. B. Zhang, Nano Energy **16**, 488 (2015).
19. J. Xu, Z. Q. Tan, W. C. Zeng, G. X. Chen, S. L. Wu, Y. Zhao, K. Ni, Z. C. Tao, M. Ikram, H. X. Ji, and Y. W. Zhu, Adv. Mater. **28**, 5222 (2016).
20. K. Zhang, L. Mao, L. L. Zhang, H. S. O. Chan, X. S. Zhao, and J. S. Wu, J. Mater. Chem. **21**, 7302 (2011).
21. B. Zhao, P. Liu, Y. Jiang, D. Y. Pan, H. H. Tao, J. S. Song, T. Fang, and W. W. Xu, J. Power Sources **198**, 423 (2012).
22. D. F. Yang and C. Bock, J. Power Sources **337**, 73 (2017).
23. W. Gao, N. Singh, L. Song, Z. Liu, A. L. M. Reddy, L. J. Ci, R. Vajtai, Q. Zhang, B. Q. Wei, and P. M. Ajayan, Nat. Nanotechnol. **6**, 496 (2011).
24. M. F. El-Kady, V. Strong, S. Dubin, and R. B. Kaner, Science **335**, 1326 (2012).
25. D. Wu, Q. D. Chen, H. Xia, J. Jiao, B. B. Xu, X. F. Lin, Y. Xu, and H. B. Sun, Soft Matter **6**, 263 (2010).
26. H. B. Jiang, Y. L. Zhang, D. D. Han, H. Xia, J. Feng, Q. D. Chen, Z. R. Hong, and H. B. Sun, Adv. Funct. Mater. **24**, 4595 (2014).